JOURNAL OF APPLIED PHYSICS **115**, 054906 (2014)

Phosphorus vacancy cluster model for phosphorus diffusion gettering of metals in Si

Renyu Chen, Bart Trzynadlowski, and Scott T. Dunham
Department of Electrical Engineering, University of Washington, Seattle, Washington 98195, USA

(Received 26 October 2013; accepted 24 January 2014; published online 6 February 2014)

In this work, we develop models for the gettering of metals in silicon by high phosphorus concentration. We first performed *ab initio* calculations to determine favorable configurations of complexes involving phosphorus and transition metals (Fe, Cu, Cr, Ni, Ti, Mo, and W). Our *ab initio* calculations found that the P_4V cluster, a vacancy surrounded by 4 nearest-neighbor phosphorus atoms, which is the most favorable inactive P species in heavily doped Si, strongly binds metals such as Cu, Cr, Ni, and Fe. Based on the calculated binding energies, we build continuum models to describe the P deactivation and Fe gettering processes with model parameters calibrated against experimental data. In contrast to previous models assuming metal-P_1V or metal-P_2V as the gettered species, the binding of metals to P_4V satisfactorily explains the experimentally observed strong gettering behavior at high phosphorus concentrations. © *2014 AIP Publishing LLC*. [http://dx.doi.org/10.1063/1.4864377]

I. INTRODUCTION

Transition metals, such as Fe, Cu, Cr, Ni, Ti, Mo, and W, have detrimental effects on silicon device performance. Many transition metals are fast diffusers in silicon, with diffusivities many orders of magnitude larger than common dopants.[1] For this reason, metal contaminants can diffuse and redistribute throughout the whole wafer. Dissolved metals often possess many deep energy levels and are thus effective generation-recombination centers that deteriorate carrier lifetime.[2] This can limit the efficiency of silicon solar cells and increases the noise level of CMOS image sensors.

Gettering is a common approach in both microelectronics and silicon photovoltaics to minimize harm due to transition metal contaminants by removing them from the active device region. Phosphorus diffusion gettering is of particular interest in silicon photovoltaics as it occurs during the fabrication of functional parts of cells (e.g., emitter of *p*-type cell). It is well known that high phosphorus concentrations can getter interstitial metals, but the fundamental mechanism has not been clearly determined. It is thus crucial to develop predictive models incorporating important atomic processes during gettering, such that various processing conditions can be explored for optimum gettering efficiency.

In this work, we combine *ab initio* and continuum approaches to investigate critical atomic processes during phosphorus diffusion gettering of Fe. As phosphorus diffusion gettering usually occurs under high P concentrations, we first performed *ab initio* calculations to determine possible phosphorus configurations under heavy doping and the binding of metal atoms to these P containing complexes. We then build continuum models to simulate the gettering of iron under high phosphorus concentration. The simulated iron profile and gettering kinetics agree well with experimental data.

II. *AB INITIO* CALCULATIONS OF PHOSPHORUS AND METAL COMPLEXES IN Si

A. Computational details

All the *ab initio* calculations were done using the density functional theory (DFT) code VASP[3,4] with the Perdew-Wang 1991 generalized gradient approximation (GGA) functional[5] and ultrasoft Vanderbilt-type pseudopotentials.[6,7] Calculations are performed in a supercell consisting of 64 lattice sites with a $2 \times 2 \times 2$ mesh of Monkhorst-Pack[8] *k*-points for integrations over the Brillouin zone, and a 320 eV cutoff in the plane-wave expansions. The GGA equilibrium lattice constant was used and kept fixed throughout the calculations. Energy gain due to stress relaxation is quite small (<0.02 eV).

B. Phosphorus-vacancy complexes in P deactivation

Dopants (e.g., phosphorus, arsenic) in silicon normally occupy substitutional lattice sites. When dopant concentrations exceed solid solubility, they form complexes that are no longer electrically active. For common dopants in silicon, several models have been proposed for the deactivation mechanism. Deactivation of arsenic in silicon is known to be dominated by the vacancy cluster mechanism based on both theoretical and experimental evidence.[9–14] The deactivation mechanism of phosphorus is still under debate due to the lack of conclusive experimental observations. While some propose the formation of SiP precipitates as the major deactivation mechanism,[15] others suggest a vacancy cluster model similar to arsenic deactivation based on the similarities of phosphorus and arsenic in silicon.[16,17] In the vacancy cluster model, phosphorus deactivates through the formation of phosphorus-vacancy clusters, each containing up to 4 phosphorus atoms and a vacancy. These clusters can be written as P_nV, denoting a vacancy paring with n of its nearest phosphorus neighbors ($1 \leq n \leq 4$). Figure 1 illustrates the

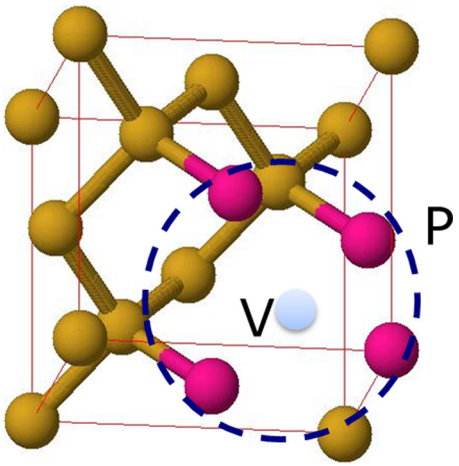

FIG. 1. Schematic of a P_4V cluster containing 4 phosphorus atoms (pink/dark) and a vacancy (grey/light). Yellow spheres denote silicon atoms.

structure of a P_4V cluster. We have performed *ab initio* total energy calculations that further support the vacancy cluster model.

The formation energies of the clusters are extracted from the calculated total energy values and are listed in Table I. The formation energy of P_nV is referenced to neutral substitutional phosphorus and bulk silicon:

$$E^f_{P_nV} = E^{tot}_{P_nV} - nE^{tot}_{P_S} + \left(n - \frac{63}{64}\right)E^{tot}_{Si}, \tag{1}$$

where $E^{tot}_{P_nV}$, $E^{tot}_{P_S}$, and E^{tot}_{Si} denote the calculated total energies of the P_nV cluster, substitutional phosphorus, and 64-atom bulk silicon, respectively. n can vary from 0 to 4, where $n = 0$ corresponds to a single vacancy. In this work, we are dealing with very high phosphorus concentrations such that the donor bands overlap with the conduction band minimum, and the Fermi level sits in this merged band. Thus, we use neutral substitutional phosphorus rather than P_S^+ as the energy reference.

The formation energy is a measure of the stability of the defect, with lower values indicating higher stability. Due to the large binding between phosphorus and vacancy, the formation energy of P_nV decreases monotonically as more P atoms are incorporated. This causes negative formation energies of P_3V and P_4V, indicating that the formation of P_nV is exothermic for $n \geq 3$. The average of the energy gain of adding a phosphorus to an existing P_nV, which is simply the differences of formation energy values between adjacent columns of Table I, is around 1.3 eV.

Based on the above *ab initio* calculations, we use thermodynamics to estimate the equilibrium concentrations of various phosphorus species as functions of the total phosphorus concentration. The equilibrium concentration of the clusters are calculated by

$$C_{P_nV} = C_{Si}\left(\frac{C_{P_S}}{C_{Si}}\right)^n\left(\frac{C_V}{C^*_V}\right)\exp\left(-\frac{G^f_{P_nV}}{kT}\right), \tag{2}$$

where $G^f_{P_nV}$ is the Gibbs free energy of formation of the P_nV cluster. Neglecting formation entropy changes, $G^f_{P_nV}$ is equal to the formation energy $E^f_{P_nV}$ as defined in Eq. (1). C_{Si} is the silicon lattice density ($5 \times 10^{22}\,cm^{-3}$). C_V and C^*_V are the actual and equilibrium vacancy concentrations, respectively; the ratio between the two is a measure of the vacancy supersaturation. The total phosphorus concentration is, thus, is given as

$$C^{tot}_P = C_{P_S} + n\sum_{n=1}^{4} C_{P_nV}. \tag{3}$$

For a given temperature and vacancy supersaturation condition, we can solve concentrations of all phosphorus species as functions of the total phosphorus concentration C^{tot}_P using Eqs. (2) and (3), as plotted in Figure 2 under equilibrium vacancy concentrations ($C_V = C^*_V$) and at a temperature of 840 °C, a common temperature for the phosphorus emitter diffusion process. At this temperature, when the total phosphorus concentration is low ($<10^{20}\,cm^{-3}$), virtually all phosphorus atoms take the substitutional form. For total P concentrations exceeding $10^{20}\,cm^{-3}$, the concentration of P_4V increases steeply and quickly becomes comparable to that of P_S. When the total P concentration further increases, P_4V becomes the dominant species, while the active phosphorus concentration remains at around $2 \times 10^{20}\,cm^{-3}$. For all concentration ranges, the concentrations of P_nV with $n \leq 3$ are negligible and thus do not show up in the plot. Our *ab initio* calculations find P_4V to be neutral for all Fermi levels within the band gap, suggesting that P_4V is the dominant inactive phosphorus species. The above analysis is consistent with experimental observations on the dependencies of

TABLE I. Formation energies of neutral P_nV clusters and a neutral vacancy, referenced to neutral substitutional phosphorus and bulk silicon.

Structure	V	PV	P_2V	P_3V	P_4V
E^f (eV)	3.50	2.31	0.97	−0.18	−1.68

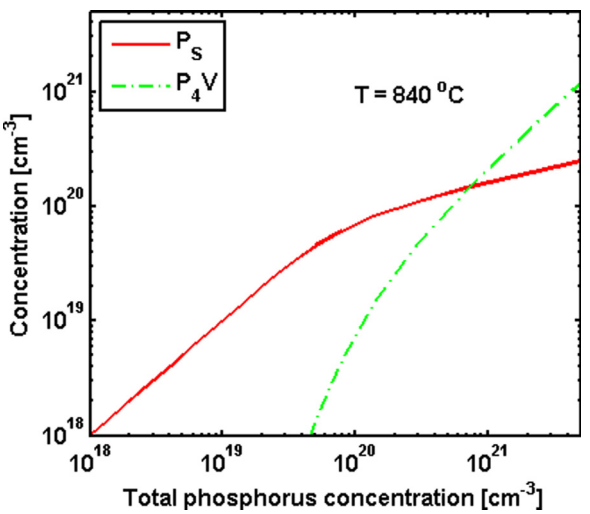

FIG. 2. Equilibrium substitutional phosphorus P_S (active) concentration and P_4V (inactive) concentration as functions of the total phosphorus concentration at 840 °C. The concentrations of P_nV with $n \leq 3$ are negligible and fall out of the plotting range.

TABLE II. Formation energies (unit: eV) of neutral M-P_nV complexes, referenced to neutral tetrahedral metal interstitials (M_I), substitutional phosphorus, and bulk silicon. M_I-P_S corresponds to an interstitial metal paired with a substitutional phosphorus. M-V corresponds to a metal occupying the vacant site, which is simply a substitutional metal (M_S). M-P_nV corresponds to a substitutional M bonding with n phosphorus atoms.

Metals (M)	M_I-P_S	M-V (M_S)	M-P_1V (PM)	M-P_2V (P_2M)	M-P_3V (P_3M)	M-P_4V (P_4M)
Fe	−0.02	0.56	−0.44	−1.47	−2.48	−3.20
Cu	−0.07	0.34	−0.94	−2.19	−3.37	−4.03
Cr	−0.22	0.30	−0.80	−1.50	−2.41	−3.67
Mo	0.01	0.89	−0.10	−1.31	−1.98	−2.57
Ni	−0.10	0.50	−0.52	−1.59	−2.52	−3.60
Ti	−0.08	0.77	−0.26	−1.41	−2.30	−3.21
W	0.09	0.60	−0.39	−1.57	−2.23	−2.90

active and inactive phosphorus concentrations on the total phosphorus concentration,[18] although a much higher P concentration (above $10^{21}\,cm^{-3}$) may also lead to SiP precipitates.

C. Phosphorus-vacancy-metal complexes in metal gettering

To investigate the mechanism of phosphorus diffusion gettering of metal, we have also calculated the total energies of a metal atom paired with the vacancy and clusters. We find that the lowest energy structure for the metal atom, denoted by M, to incorporate into the P_nV structures are for M to occupy the vacancy site. The formation energies of a given complex containing M and P are referenced to neutral tetrahedral M interstitial (the most stable configuration in n-type Si), neutral substitutional phosphorus and bulk silicon

$$E^f_{\mathrm{M-P}_n\mathrm{V}} = E^{tot}_{\mathrm{M-P}_n\mathrm{V}} - E^{tot}_{\mathrm{M_I}} - nE^{tot}_{\mathrm{P_S}} + (n + 1/64)E^{tot}_{\mathrm{Si}}, \quad (4)$$

where $E^{tot}_{\mathrm{M-P}_n\mathrm{V}}$ and $E^{tot}_{\mathrm{M_I}}$ denote the calculated total energies of the M-P_nV complex and interstitial M, respectively. n can vary from 0 to 4. For example, $n = 0$ (M-P_0V) corresponds to a substitutional M (M_S), and $n = 1$ (M-P_1V) corresponds to a substitutional M paired with a nearest-neighbor substitutional P (PM). The formation energy values for all metal-P_nV complexes are listed in Table II and plotted in Figure 3.

From the table, we see that the formation energy of Fe-P_nV complex decreases monotonically with increasing number of P atoms. The overall energy gain for adding P atoms into the complex is smaller than the energy gain of P_nV without Fe, as indicated by the vertical spacing of symbols in Figure 3. For all metal-P_nV complexes, M-P_4V has the lowest formation energy. This and the dependences in Figure 2 suggest the dominance of M-P_4V under high P concentrations. We also find that no gap states exist for M-P_4V, further confirming that M-P_4V is a gettered inactive metal species. The calculated results, particularly those for iron, are in contrast to the assumptions of strong binding of first-nearest-neighbor substitutional iron and phosphorus.[19–22] Our DFT calculations show that Fe-P_4V has much lower formation energy than Fe-P_1V (PFe), which suggests that the tendency of iron to bind with P_4V is much stronger than that to bind with a substitutional phosphorus atom.

Mo and W have the weakest binding interactions with P_nV, possibly due to their relatively large atomic radii. Ti and Fe have moderate binding with P_nV. Cr, Ni, and Cu have strong binding to P_nV, with Cu having the strongest binding of all the metals considered. Also shown in Table II are the binding energies between interstitial metals and substitutional phosphorus (M_I-P_S), which indicate negligible (Cr, Fe, Cu, Ni, Ti) binding or repulsion (Mo, W) between interstitial metal and substitutional phosphorus atoms.

Based on Table II, we can estimate the relative concentrations of complexes in equilibrium, neglecting differences in the formation entropies. For a typical process, temperature of 840 °C and a total phosphorus concentration of 5×10^{21} cm^{-3}, the substitutional phosphorus concentration is around 2.3×10^{20} cm^{-3} according to Fig. 2. The calculated equilibrium ratios of $C_{\mathrm{M_I-P_S}}$, $C_{\mathrm{Fe-PV}}$, and $C_{\mathrm{Fe-P_2V}}$ to $C_{\mathrm{Fe-P_4V}}$ are 4×10^{-8}, 3×10^{-6}, and 7×10^{-4}, respectively, indicating that Fe-P_4V is the dominant species at high phosphorus concentrations.

III. CONTINUUM MODELS FOR P DEACTIVATION AND Fe GETTERING

Based on the *ab initio* calculations, we have built continuum models to describe the P deactivation and Fe gettering processes. P deactivation occurs via formation of clusters[23]

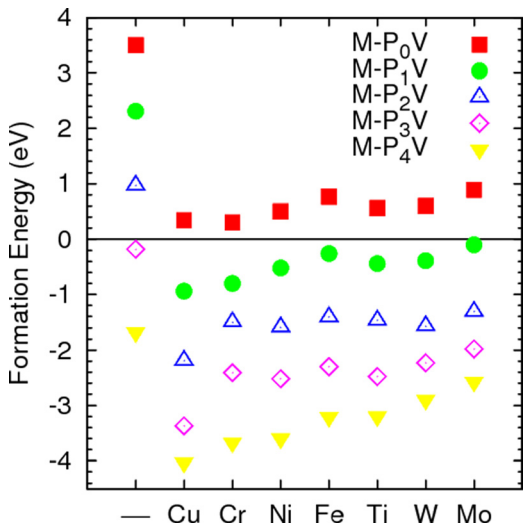

FIG. 3. Formation energies (eV) of various metal-P_nV clusters. The first column corresponds to pure P_nV without metal atoms.

$$V + P_S \Longleftrightarrow PV, \tag{5a}$$

$$PV + P_S \Longleftrightarrow P_2V, \tag{5b}$$

$$PV + PV \Longleftrightarrow P_2V + V, \tag{5c}$$

$$PV + P_2V \Longleftrightarrow P_3V + V, \tag{5d}$$

$$PV + P_3V \Longleftrightarrow P_4V + V, \tag{5e}$$

where P_S is the substitutional active phosphorus. We assume that only V and PV are mobile species. A vacancy, when encountering a P_S, can form a mobile PV pair. The PV pair can bind with either P_S or another PV to form P_2V. Then, PV can further migrate and react with P_2V and P_3V to form P_3V and P_4V, respectively. The clustering reactions terminate at P_4V as there are no more nearest neighbor sites of the V to be occupied by P atoms.

The reaction rates are defined as

$$R_{V/P_S} = 4\pi a \cdot d_V\left(C_V C_{P_S} - K_{V/P_S} \cdot C_{PV}\right), \tag{6a}$$

$$R_{PV/P_S} = 4\pi a \cdot d_{PV}\left(C_{PV} C_{P_S} - K_{PV/P_S} \cdot C_{P_2V}\right), \tag{6b}$$

$$R_{PV/PV} = 4\pi a \cdot 2d_{PV}\left(C_{PV} C_{PV} - K_{PV/PV} \cdot C_{P_2V} C_V\right), \tag{6c}$$

$$R_{PV/P_2V} = 4\pi a \cdot d_{PV}\left(C_{PV} C_{P_2V} - K_{PV/P_2V} \cdot C_{P_3V} C_V\right), \tag{6d}$$

$$R_{PV/P_3V} = 4\pi a \cdot d_{PV}\left(C_{PV} C_{P_3V} - K_{PV/P_3V} \cdot C_{P_4V} C_V\right), \tag{6e}$$

where the K terms are equilibrium constants that are only functions of temperature, d is the diffusivity of the model species, and a is the capture cross section of the reactions. These constants contain Arrhenius terms with activation energies that are directly extracted from *ab initio* calculations as in Tables I and II. The prefactors of these terms contain additional entropy factors that are neglected in the previous equilibrium thermodynamics analysis and are used as fitting parameters.

As P_4V and FeP_4V are dominant species under high P concentrations, the phosphorus diffusion gettering mechanism can be simply described by the reaction

$$Fe_I + P_4V \Longleftrightarrow FeP_4V, \tag{7}$$

where Fe_I is the mobile interstitial Fe. The reaction rates is defined as

$$R_{Fe_I/P_4V} = 4\pi a \cdot d_{Fe_I}\left(C_{Fe_I} C_{P_4V} - K_{Fe_I/P_4V} \cdot C_{FeP_4V}\right), \tag{8}$$

where d_{Fe_I} is the diffusivity of Fe in Si, and is set as $1.3 \times 10^{-3}\exp\left(-\frac{0.68}{kT}\right)$ cm^2s^{-1} from Ref. 26. a is the capture cross section of the reacting species with a typical value of 0.5 nm. $K_{Fe_I/P_4V} = 4.32 C_{Si} \cdot \exp\left(\frac{1.52\ eV}{kT}\right)$, where C_{Si} is the silicon lattice density. The activation energy of 1.52 eV is simply the magnitude of the binding energy between Fe_I and P_4V, as determined by the difference of formation energies of FeP_4V and P_4V. The formation energy of Fe_I is set to 0 as it is the reference species. The prefactor in K_{Fe_I/P_4V} is related to the entropy change during binding and is used here as a fitting parameter. Its value is optimized to achieve the minimum difference between simulated and SIMS Fe profiles.

We have combined the above models with previously published phosphorus pair diffusion models[24] to simulate the phosphorus diffusion gettering process. As in Ref. 24, the dominating species for the phosphorus vacancy pair is assumed to be $(PV)^-$, whose diffusivity $D_{(PV)^-}$ is proportional to $C_{P^+}^2$ under high doping concentrations.

We have performed simulations on phosphorus diffusion gettering experiments of Fe in monocrystalline Si in the range of 650–800 °C.[21] Phosphorus is diffused into Si from a doped oxide layer. The diffusivity of P in the doped-oxide is set as $2.15 \times 10^{-9}\exp\left(-\frac{1.71}{kT}\right)$ cm^2s^{-1}, as reported in Ref. 25. We did not include segregation of Fe into the SiO_2 surface as simulations in Ref. 19 suggest that the Fe dose that is segregated into SiO_2 is only a negligible amount of the total Fe dose. We have simulated the resulting P (both total and active) and Fe profiles under in-diffusion of 30 min at 870 °C followed by an anneal of 2 h at 800 °C. The simulated profiles are in close agreement with experimental findings, as shown in Figure 4. The difference between total (solid red) and active (dashed blue) phosphorus is roughly 4 times the P_4V concentration. P_4V dominates in the region at the first 0.1 μm, and Fe atoms are attracted to this region due to the strong binding of Fe and P_4V. It is evident in Fig. 4 of Ref. 19 that the model assuming Fe-P_1V predicts a linear relation between P and Fe concentrations towards regions with high phosphorus concentration, a much weaker gettering behavior. In contrast, our calculated gettered profiles based on Fe-P_4V show the experimentally observed strong and nonlinear gettering behavior: the faster increase of Fe concentration towards surface compared to that of P.

Like Fe,[21] experimentally observed gettering behaviors of Cr,[27] and Co[28] show a very rapid drop of gettered metal concentration as phosphorus concentration decreases, suggesting a strongly super-linear relationship between phosphorus and gettered metal concentrations. Ref. 28 assumes the formation of P_2Co complexes, but an even stronger dependence of segregation on P concentration as for neutral

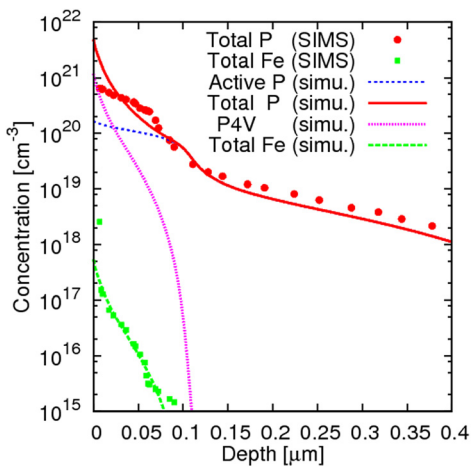

FIG. 4. Simulated Fe and P profiles after annealing compared to SIMS data, Ref. 21 (in-diffusion of 30 min at 870 °C followed by anneal of 2 h at 800 °C).

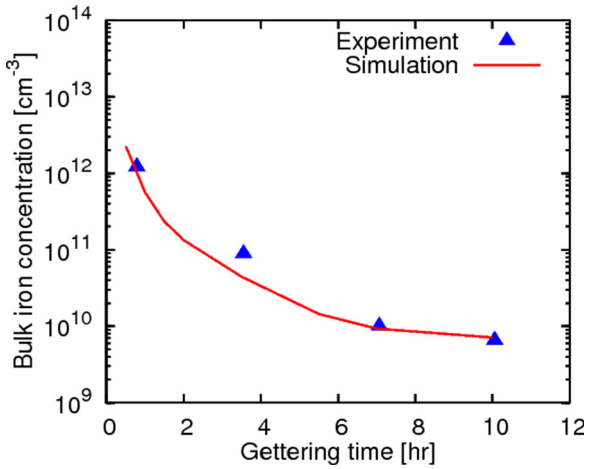

FIG. 5. Simulated bulk interstitial iron concentration at various stages of a gettering compared to experimental data from Ref. 21 (in-diffusion at 870 °C for 30 min, then a ramp-down to 650 °C for 90 min, followed by annealing at 650 °C for 8 h).

Co-P_4V (P_4Co) would be more consistent with the experimentally observed data shown in Fig. 1 of Ref. 28. These are all consistent with our model that suggests metal-P_4V as the gettered species.

We also simulated gettering kinetics at various stages of a gettering experiment: in-diffusion at 870 °C for 30 min, then a ramp-down to 650 °C for 90 min, followed by an anneal at 650 °C for 8 h. The simulated bulk iron concentrations match closely with experimental data, as shown in Figure 5.

The model can be readily used for gettering at other temperatures, as the K parameters are all temperature dependent (Arrhenius). Temperature affects gettering through multiple factors: (a) Eq. (8) gives a decrease in gettering due to retarded Fe-P_4V formation as temperature increases; (b) the formation of P_4V could be reduced at higher temperature according to equation set (6), which also retards gettering; and (c) phosphorus in-diffusion may increase at higher temperature, causing a net increase in total amount of P, thus increasing gettering. The actual gettering efficiency is determined by the relative strengths of all above factors, which cause the temperature dependence to have multiple regimes. This qualitatively agrees with the observations in Ref. 29, where a complicated temperature dependence of gettering behavior is observed. In that reference, an increase in gettering efficiency is observed from 748 °C to 920 °C, suggesting that the in-diffusion mechanism (c) plays a dominant role. After 943 °C, we see a decrease in gettering efficiency, suggesting that we are in the binding limited regime, where (a) and (b) are dominant. Note that in Ref. 29, the total dose of Fe is not conserved for various temperatures, making quantitative comparison impossible.

Assuming total phosphorus concentration is unchanged, then (a) and (b) become the dominant mechanism to affect gettering. In this case, low temperature anneal is actually beneficial to gettering. This agrees with experimental observations in Ref. 30, where a low temperature annealing tail increases gettering efficiency.

IV. CONCLUSIONS

In this work, we developed models to account for phosphorus diffusion gettering of transition metals. The critical species responsible for both the P deactivation and metal gettering processes is identified to be the P_4V complex, and the dominant gettered species is M-P_4V, with the metal atom sitting in the vacant site. Continuum models for gettering of iron under high phosphorus concentrations were built based on *ab initio* calculations and critical model parameters were further calibrated against experimental data. The continuum simulations can be easily extended to other metals to explore various processing conditions during device fabrication to optimize gettering efficiency and the resulting device performance.

ACKNOWLEDGMENTS

This work was partially funded by support from Silicon Solar Consortium (SiSoC), Silicon Wafer Engineering and Defect Science (SiWEDS) and Sony Corporation. A portion of the research was performed using EMSL, a user facility sponsored by the Department of Energy's Office of Biological and Environmental Research.

[1]J. D. Plummer, M. D. Deal, and P. B. Griffin, *Silicon VLSI Technology: Fundamentals, Practice, and Modeling* (Prentice Hall, Upper Saddle River, NJ, 2000).
[2]A. A. Istratov, H. Hieslmair, and E. R. Weber, Appl. Phys. A **70**, 489 (2000).
[3]G. Kresse and J. Hafner, Phys. Rev. B **47**, 558 (1993).
[4]G. Kresse and J. Furthmuller, Phys. Rev. B **54**, 11169 (1996).
[5]J. P. Perdew, J. A. Chevary, S. H. Vosko, K. A. Jackson, M. R. Pederson, D. J. Singh, and C. Fiolhais, Phys. Rev. B **46**, 6671 (1992).
[6]D. Vanderbilt, Phys. Rev. B **41**, 7892 (1990).
[7]G. Kresse and J. Hafner, J. Phys.: Condens. Matter **6**, 8245 (1994).
[8]H. J. Monkhorst and J. D. Pack, Phys. Rev. B **13**, 5188 (1976).
[9]R. B. Fair and G. R. Weber, J. Appl. Phys. **44**, 273 (1973).
[10]E. Guerrero, H. Potzl, R. Tielert, M. Grasserbauer, and G. Stingeder, J. Electrochem. Soc. **129**, 1826 (1982).
[11]D. Nobili, S. Solmi, M. Merli, and J. Shao, J. Electrochem. Soc. **146**, 4246 (1999).
[12]K. C. Pandey, A. Erbil, G. S. Cargill, R. F. Boehme, and D. Vanderbilt, Phys. Rev. Lett. **61**, 1282 (1988).
[13]M. Ramamoorthy and S. T. Pantelides, Phys. Rev. Lett. **76**, 4753 (1996).
[14]P. M. Rousseau, P. B. Griffin, W. T. Fang, and J. D. Plummer, J. Appl. Phys. **84**, 3593 (1998).
[15]S. Solmi, A. Parisini, R. Angelucci, A. Armigliato, D. Nobili, and L. Moro, Phys. Rev. B **53**, 7836 (1996).
[16]Y. Takamura, S. H. Jain, P. B. Griffin, and J. D. Plummer, J. Appl. Phys. **92**, 230 (2002).
[17]Y. Takamura, P. B. Griffin, and J. D. Plummer, J. Appl. Phys. **92**, 235 (2002).
[18]P. Pichler, *Intrinsic Point Defects, Impurities, and Their Diffusion in Silicon* (Springer, Wien, New York, 2004).
[19]J. Schön and W. Warta, in *Proceedings of the 24th European Photovoltaic Solar Energy Conference* (WIP, Valencia, Spain, 2008), pp. 1851–1854.
[20]A. Haarahiltunen, H. Savin, M. Yli-Koski, H. Talvitie, and J. Sinkkonen, J. Appl. Phys. **105**, 023510 (2009).
[21]H. Talvitie, V. Vahanissi, A. Haarahiltunen, M. Yli-Koski, and H. Savin, J. Appl. Phys. **109**, 093505 (2011).
[22]V. Kveder, W. Schröter, A. Sattler, and M. Seibt, Mater. Sci. Eng., B **71**, 175 (2000).
[23]H. Wagner, A. Dastgheib-Shirazi, R. Chen, S. T. Dunham, and P. P. Altermatt, in Proceedings of 2011 IEEE Photovoltaics Specialist Conference (Seattle, 2011).

[24]S. T. Dunham, J. Electrochem. Soc. **139**, 2628 (1992).
[25]G. F. Cerofolini, M. L. Polignano, P. Picco, M. Finetti, S. Solmi, and M. Gallorini, Thin Solid Films **87**, 373 (1982).
[26]E. R. Weber, Appl. Phys. A **30**, 1 (1983).
[27]N. Khelifati, D. Bouhafs, M. Boumaour, S.-E.-H. Abaidia, and B. Palahouane, Mater. Sci. Semicond. Process. **15**, 56 (2012).
[28]W. Schröter, V. Kveder, M. Seibt, A. Sattler, and E. Spiecker, Sol. Energ. Mater. Sol. Cells. **72**, 299 (2002).
[29]M. Syre, S. Karazhanov, B. R. Olaisen, A. Holt, and B. G. Svensson, J. Appl. Phys. **110**, 024912 (2011).
[30]V. Vähänissi, A. Haarahiltunen, H. Talvitie, M. Yli-Koski, and H. Savin, Prog. Photovolt.: Res. Appl. **21**, 1127 (2013).